Lithographic Patterning and Etching of Hafnium Oxide Metasurfaces

Remi Dado, Priyanuj Bordorloi
Mentors: Usha Raghuram, Vijay Narasimhan, Swaroop Kommera
E241 Spring 2024

Table of Contents:

1. Introduction and Benefits:

1.1 Introduction:

Arrays of subwavelength-scale nanodisks demonstrate unique abilities to participate in or enhance a range of light-matter interactions. Illumination of certain metasurfaces with circularly polarized light can enhance optical chirality *C*, a measure of electromagnetic field asymmetry. Work on metasurfaces active in the infrared and near-infrared range have demonstrated enhancement of circular dichroism signal for high-resolution spectroscopy, chirally-selective photoionization, and preferential 'trapping' of one enantiomer over another.[1] However, many of these simulated effects are yet to be experimentally demonstrated; alternatively, spectral alignment of resonance frequencies could magnify several more subtle, but experimentally demonstrated effects. Many organic molecules demonstrate optical activity in this 100-400 nm range; producing this chiral-field enhancement in the ultraviolet (UV) range, rather than the previously demonstrated (near)-infrared window, would open applications in enantiomeric separation and enantioselective chemical synthesis.[1,2] Hafnium oxide, a high-refractive index, lossless dielectric in the UV range, is a promising material for UV-resonant metasurfaces that potentially enhance these weak light-matter interactions.

Enhancing chiral light-matter interactions facilitates the study of many intricate photonic, physical, and chemical properties. Simultaneously, significant enhancement and functionalization could address current inefficiencies in industrial chemical synthesis. The chirality, or 'handedness', of molecules can strongly dictate a compound's activity, efficiency, and safety. Though not all bioactive compounds contain stereogenic centers, chiral molecules now compose more than a third of agrochemicals and more than half of pharmaceuticals.[3] As such, the biomedical, agricultural, and chemical industries all employ techniques to manipulate the 'handedness' of products, dedicating considerable time and resources to isolating a particular isomer.[3] The high cost associated with separation and/or asymmetric synthesis procedures leads commercial markets to predominantly sell racemic mixtures: over 90% of chiral molecules are sold as such, despite environmental and biomedical disadvantages, including adverse side effects and delayed onset times in pharmaceuticals and increased dispersion and aquatic toxicity in agrochemicals.[2] Developing more facile methods for stereoselective reactions and separations could bring more effective medications to the public, enable agile response to agrochemical crises, and increase supply chain efficiency for essential chemical production. Simultaneously, UV-resonant metasurfaces represent rich opportunities for the study of 2D transition metal dichalcogenides, valley polarization, and quantum materials.[4]

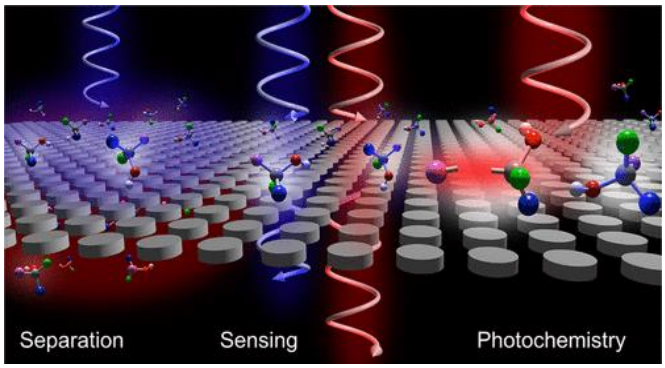

Image 1. Adaptation of chiral-field enhancing metasurfaces to the UV range opens many applications.[1]

Our project goal was the development of a reliable process flow for fabricating HfO_2 metasurfaces. To do so, we established patterning schemes using HSQ and Al_2O_3 as hard masks for pattern transfer through electron beam lithography (EBL) and inductively coupled plasma reactive ion (ICP RIE) etching. The RF magnetron sputtering deposition and etching recipes developed throughout the course provide clear starting points for further hafnia metasurface fabrication and generalizable processes for construction of other comparably sized structures. The conditions and process flow established successfully produce patterned HfO_2 structures on the order of magnitude intended. Moving forward, the

structural precision of these nanodisks can be improved through tuning the etching and e-beam parameters. Specifically, minimizing over-etching and optimizing the electron beam dosage are immediate future steps for more highly anisotropic patterning, essential to robust, tunable optical behavior.

1.2 Benefit to SNF community:

Outside of chiral and optical applications, this project constitutes a foundation for broadly applicable, top-down fabrication of hafnium oxide nanostructures. In addition to its desirability as an optical dielectric, hafnia has become an increasingly key component of microelectronic and other device manufacturing. Hanfia's dielectric index and band gap permit its use in dynamic random access memory capacitors, metal–oxide–semiconductor devices, resistive-switching memories, and CMOS-compatible ferroelectric field-effect transistors, among other applications. Given the breadth of interest, a reliable process for nano-scale HfO_2 patterning serves the general interest of the SNF community. SNF's position at the intersection of industry, academia, and government research motivates the development of robust processes for working with and characterizing such an agile, characteristically valuable material.

In addition to the direct benefits of an overall scheme for nano-scale patterning of HfO_2, developing such a process produces a useful body of engineering information for common cleanroom techniques and other materials, namely hydrogen silsesquioxane (HSQ) and aluminum(III) oxide, Al_2O_3. RF sputtering of hafnia and especially alumina are key steps in many devices and samples assembled in SNF, making reliable, relatively optimized recipes for film deposition valuable to many users. Similarly, reactive-ion dry etching, specifically inductively coupled plasma-reactive ion etching in the PT-MTL tool, remains popular and broad characterization data regarding rates and selectivity could permit users to more easily adjust recipes for their own projects. In conjunction with SNF tools and processes, the lithography process is characterized using scanning electron microscopy (SEM) in the SNSF. Information about the resolution and directionality of patterning through EBL and subsequent etching steps knits together resources from across campus to most effectively produce high-quality structures on this scale.

2. Processing and Methods

2.1 Structure design:

Our plan was to fabricate hafnia nano-disks on a quartz substrate, which provides a good refractive index contrast for light confinement: an important parameter for such metasurfaces (Figure 1). We patterned these disks using an alumina hard etch mask in F-based chemistry. The alumina hard mask itself is patterned through EBL (specifically with EBPG) using 6% HSQ as a negative-tone e-beam resist. HSQ will pattern planar features of the hafnia structure (i.e. radius and lattice features), while the thickness of the deposited Hafnia film would dictate the height of the disks. Then, Cl-based etch would transfer the developed HSQ pattern onto the alumina.

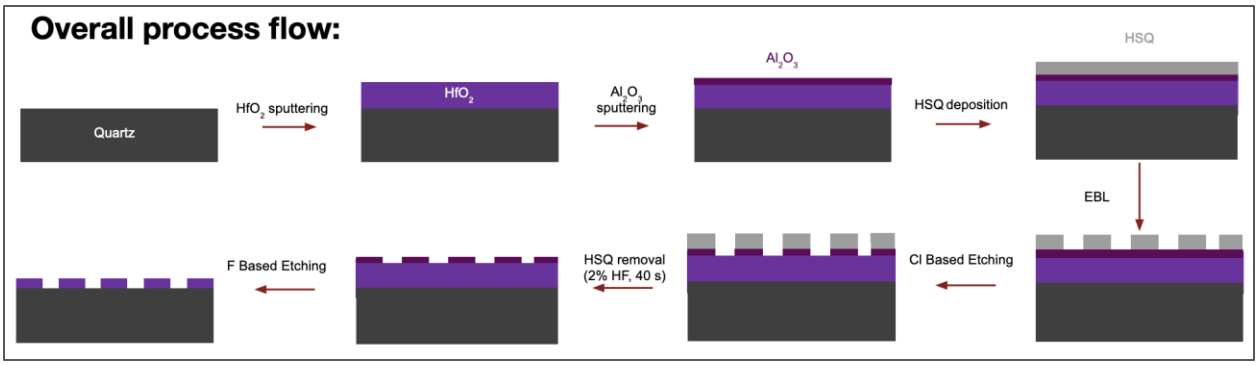

Figure 1. Overall process flow to make hafnia metasurfaces; disks are not drawn to scale.

To determine the required thickness of the hafnia film, we used a finite-element method solver (COMSOL) to find disk parameters that exhibit electric and magnetic-dipole Mie resonances in the far to mid-UV wavelength regime. These resonances can be characterized by their sharp decrease in the structure's transmittance values and a large increase in a parameter labeled C/C_{CPL}, which measures the density of optical chirality of incoming CPL (Figure 2.).

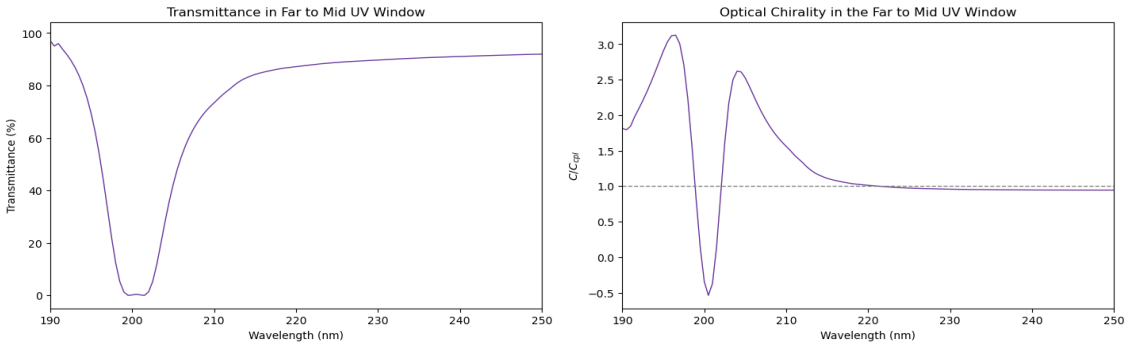

Figure 2. Optical chirality and transmission in the UV window for a periodic array of simulated nanodisks; nanodisk parameters shown in Figure 3.

Our FEM simulations indicated that for a resonance in the UV regime, the required thickness of the hafnia film will be ~ 40 nm, and therefore the corresponding thickness of alumina and HSQ would be calculated by our etch rate analysis made in the next section of this report (Figure 3).

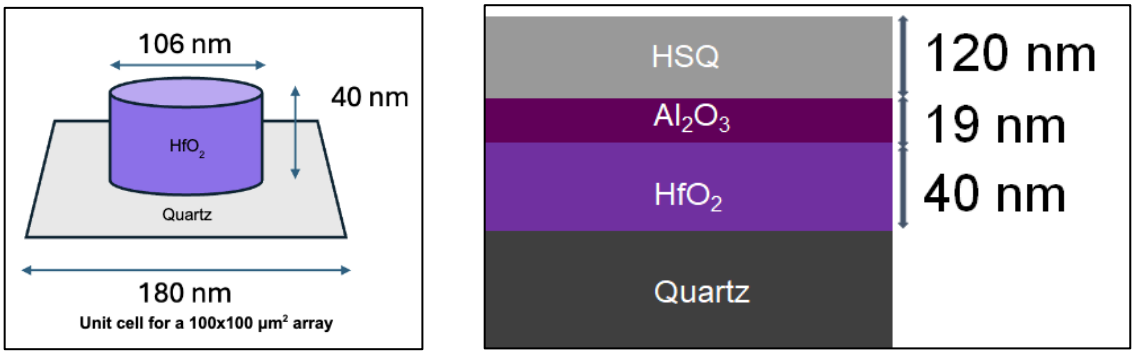

Figure 3. Lattice parameter, height, and diameter of target hafnia nanodisk (left) and assembled stack with target layer thicknesses (right).

2.2 Deposition:

Stoichiometric hafnia and alumina films were deposited using Physical Vapor Deposition (PVD) through RF magnetron sputtering with their respective targets in *Lesker2*. Before any deposition, we clean our wafers (substrates) in a piranha solution (H_2SO_4:H_2O_2 = 9:1) heated at 120^o C for 20 minutes to remove any organic contaminants.

Prior to assembling the stack, we deposited both these oxides on separate 4-inch silicon wafers. This permits reliable thickness measurements on the ellipsometer, as quartz almost fully transmits UV, visible, and NIR light. Further, we wrote thin lines (1 mm x 1 cm) using a Sharpie marker, which act as an easily removable mask during deposition. Post-deposition, washing in acetone and isopropyl alcohol (IPA) removes the Sharpie line, creating a step between the substrate and deposited material. A profilometer scan of this profile reports the thickness of the deposited layer, providing a way to calibrate and confirm ellipsometer measurements.

Deposition Parameters	**HfO_2**	**Al_2O_3**
Upstream Pressure Control Initiate	15	15
Substrate Rotation Speed	20	20
Ramp and Burn in 1	100	100
Ramp and Burn in 1	60	60
Upstream Pressure Control Reduction	5	5

Table 1. Deposition parameters for both test film on Si wafer and assembled stack on quartz on Lesker2.

	HfO_2 (on Si)	**Al_2O_3 (on Si)**
Film Thickness (nm) [Ellipsometry+Profilometry]	357.4	48.4
Rate (nm/min)	2.31	0.52

Table 2. The thickness of deposited material on test Si wafer on Lesker2

Hafnia films relatively had a faster deposition rate, 2.31 nm/min, than alumina, 0.52 nm (Table 2). However, the ellipsometry fit (mean-square error) remained poor for all hafnia films throughout the project, limiting the reliability of this technique for thickness measurements. These issues could emerge from phase transitions depending on the deposition method, as HfO_2 thin films are amorphous when sputter deposited at room temperature, but monoclinic and polycrystalline with increased heat.[5]

Generally, amorphous films exhibited consistent refractive indices, but polycrystalline films varied more widely, with scattering and refraction shifting with the variation in structure.[6] Therefore, we relied on profilometer measurements to measure hafnia thickness. The alumina ellipsometer fits were consistent, with MSE below ten, and aligned well with the profilometry measurements.

Finally, HSQ, was spin-coated on blank silicon chips for etch tests in Cl-based chemistry. The spin speed was 1500 rounds per minute (rpm), resulted in a 115-120 nm thick layer (measured by profilometry). Our research group has already standardized these spin-coating parameters for fabricating silicon metasurfaces. When depositing the stack, we use a piranha-cleaned quartz substrate and deposit the materials in the bottom-up order (hafnia→alumina→HSQ). Moreover, to make sure we deposited the accurate thickness of alumina and hafnia, we also placed blank silicon chips on each run so we could use those to gauge the thickness after each deposition. Given the inaccuracy of ellipsometry with a transparent substrate, these chips were used to monitor and adjust the deposition for each material to reach the intended stack parameters (Figure 3). The thickness of each layer was calculated based on the established etch rates and relative selectivity, as discussed below.

2.3 Etching:

2.3.1 Following EBL to pattern the top HSQ layer, chlorine-based etching was used to transfer the pattern to the alumina layer. Subsequently, this pattern was transferred from the alumina to the hafnia through fluorine-based etching in the same tool. HSQ was removed between the two etch steps through 40s immersion in a 2% (50:1) HF solution. This ensured that the cured HSQ would not act as a mask for the alumina through the second etching, risking some amount of unetched alumina remaining on top of the hafnia cylinders. Excess alumina would shift the dipole resonances and render the optical chirality enhancement of the hafnia nanodisk array ineffective. Moving forward, should the thickness and lattice parameters be appropriate, HSQ could serve as a hard mask alone, without an alumina layer; the advantage of a solvent removal allows some amount of the mask to survive the etching, entirely protecting the top of the cylinder or feature and then be removed cleanly. This removes the need for precisely calculating alumina's etch rates, where even a small miscalculation or prior mismeasurement could either leave excess on top or in the valleys of the hafnia nanodisks or overetch into the hafnia, distorting the target structure's geometry. Etch conditions can be tuned around producing vertical sidewalls, with more insurance that at least the top profile would be maintained.

However, an adaptable hafnia patterning process maintains the need for an alumina hard mask. The thickness of the hafnia nanodisks determines the main etch time and other parameters considered in the recipe development. If the target structures require a long or abrasive enough etch to entirely degrade the HSQ layer, alumina remains a necessary component. Our original target structures were 350 nm tall, which the 115-120 nm of HSQ would be unlikely to survive. Future directions include further study about the resilience of HSQ and optimization of HSQ vs. hafnia selectivity. The ultimate trial structures were 40 nm, which could be reattempted without the alumina layer in the future.

2.3.2 Final stack parameters were determined starting with the thickness of the deposited hafnia. The relative rates of hafnia and alumina etching in the chosen F-based etch conditions then were used to determine the needed thickness of alumina. From there, the thickness of alumina determined the Cl-based etch step times. These basic calculations are summarized here:

HfO_2 thickness (nm)/HfO_2 F-based etch rate (nm/s) = F-based etch time (s)

↓

F-based etch time (s)*Al_2O_3 F-based etch rate (nm/s) = Al_2O_3 thickness (nm)

↓

Al_2O_3 thickness (nm)/Al_2O_3 Cl-based etch rate (nm/s) = Cl-based etch time (s)

Following these calculations, the measured rate of HSQ etching in Cl-based conditions was used to check that the 120 nm of HSQ would survive the Cl-based etch, ensuring both the full transfer of the pattern to the Al2O3 and the necessity of HSQ removal.

2.3.3 Chlorine based etch conditions were evaluated in HSQ and alumina, both on the test Si substrates described earlier. Comparison of Cl-based etch rates with time steps of 30 and 60 sec gave consistent rates of between 5-5.5 nm/s and 4.1-4.6 nm/s for HSQ and alumina, respectively. These rates were evaluated using both ellipsometry and profilometry. Preliminary trials with Cl-based etching etched hafnia more quickly than could be reliably measured; when main etch times were lowered to the point that any amount of hafnia survived, the time step was too close to the breakthrough step times. These trials, run with main etch times of 1.2 and 2.4 s did produce a rate of 5.5 nm/sec, evaluated primarily with ellipsometry, but remain far too limited to be considered actual etch rates and should be viewed as corresponding closer to the etching completed during the breakthrough step, if anything. Should more information about Cl-based etching for hafnia itself become of interest, thicker hafnia films could be deposited for further study. If the Cl-based etching proves capable of etching the desired hafnia thickness before entirely degrading the HSQ layer and providing a sufficiently directional patterning, this etching chemistry could be used to eliminate the alumina layer. The current deposition process for HSQ provides a consistent thickness, evaluated after EBPG, and the alumina etch rate was evaluated using a 50 nm film, permitting a measurable layer to remain on the substrate after 30-60 seconds of etching.

2.3.4 Fluorine based etch conditions were optimized for selectivity, measured as the HfO_2 etch rate divided by the Al_2O_3 etch rate. Design of experiment and executed trials centered on manipulating the ratio of Argon:CF_4 gasses and ICP:bias power (Table X).

	Pressure (mTorr)	CF4 (sccm)	Ar (sccm)	SF6 (sccm)	Main Etch Time (s)	ICP Power (W)	Bias Power (W)
40:10 CF4:Ar	10	10	40	0	60	400	50
40:20 CF4:Ar	10	20	40	0	60	400	50
25:25 CF4:Ar (60s)	20	25	25	0	60	400	50
25:25 CF4:Ar (180s)	20	25	25	0	180	400	50
20:0 CF4:Ar	20	20	0	0	60	400	50
30:10 CF4:Ar	20	30	10	0	120	400	50
45:5 CF4:Ar	20	45	5	0	120	400	50
25 W Bias Power	20	25	25	0	60	400	25
10:30 CF4:Ar	20	30	10	0	60	600	50
25:25 CF4:Ar, 600 W ICP	20	25	25	0	60	600	50
800 W ICP (120s)	20	25	25	0	120	800	50
800 W ICP (60s)	20	25	25	0	60	800	50
SF6 Recipe	10	0	5	10	30	300	50

Table 3. Summary of F-based etch conditions

The results of this series of trials are reported with the total error calculated from the uncertainty in profilometry and ellipsometry measurements and the range of values from repeat trials. It should be noted that the total error appears comparable between trials with 25:25 and 20:0 CF4:Ar ratios; one outlier run appears in the 25:25 CF4:Ar (sccm:sccm) which dramatically increases the range and standard deviation. This run was run with a thinner HfO2 film and shorter chamber cleaning step, so likely produced a significantly higher HfO2 etch rate due to physical etching from contaminants in the chamber. With this run excluded, the hafnia etch rate is reliably around 22 nm/min.

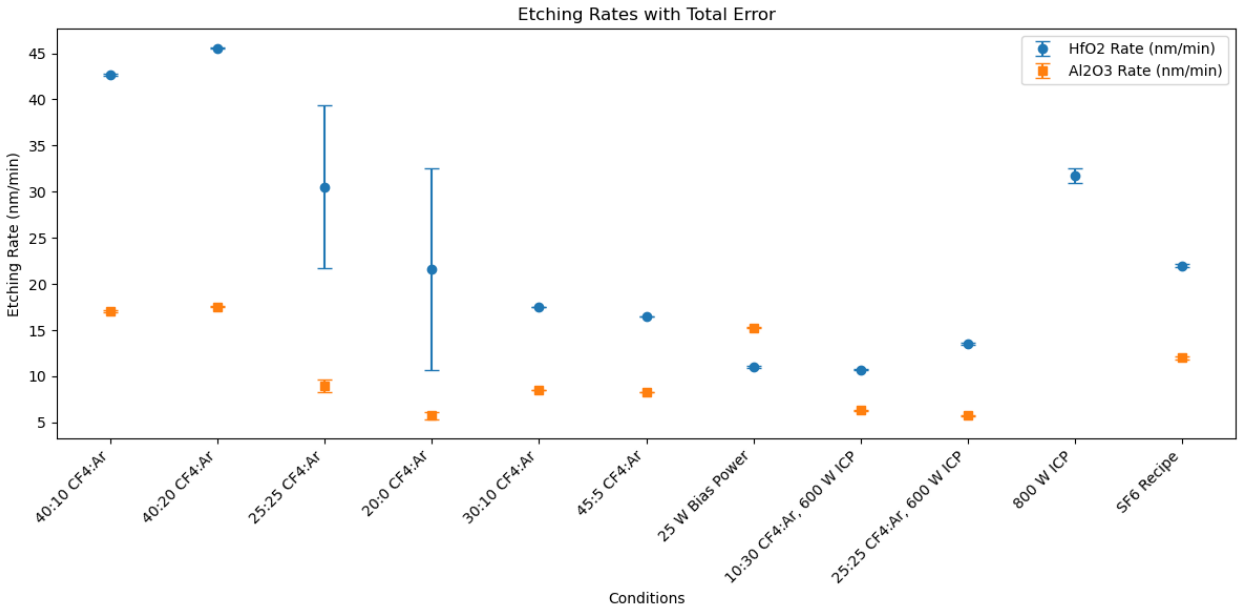

Figure 4. Hafnia and alumina etch rates in F-based conditions vary with gas ratio and ICP/bias power ratio.

Qualitatively, varying the gas ratio tuned the degree of physical etching, favored by higher Ar content, and chemical etching, caused by high concentrations of CF_4. Al_2O_3 is broadly considered inert and used as a hard mask with fluorine-based ICP RIE due to the formation of AlF_3 or alternative aluminum fluorine compounds of various stoichiometries, depending on the exact conditions.[7,8] Previous reports studying Al_2O_3 etching with CF_4 and an accompanying gas reported little dependence on the fluorine ion concentration, asserting resilience to chemical etching due to the formation of aluminum fluorine and instead a susceptibility to particle bombardment energy, more closely associated with physical etching. Results from this study loosely reflect this trend; the slowest alumina etch rates recorded occurred when no Ar was flowed into the chamber at all. However, comparably slow rates were also observed with 5, 10, and 20 sccm of Ar. This suggests with comparable, relatively low concentrations of Ar and operation in a chemical etching regime, alumina etches at a consistent, low rate, in alignment with literature reports of its behavior in Fl-based etching chemistries.[7,8]

Hafnia etch rates in Fl-based conditions showed more sensitivity to etch conditions, with gas ratios favoring chemical etching improving the selectivity (largest disparity between hafnia and alumina etch rates). Initial trials with 40:10 and 40:20 CF_4:Ar exhibited the highest rates for both oxides, but also were run with a standard cleaning step followed by a seasoning step identical to the actual etch. This is considerably shorter than the five-minute cleaning step instituted after the initial measurements, so these conditions could be repeated in the future to verify the results. When Ar was reduced to 5 sccm, keeping the overall gas flow at 50 sccm, surprisingly little selectivity was observed. This was unanticipated, given the range, including a trial with selectivity of 6.6 (hafnia etch rate/alumina etch rate), of 20:0 CF_4:Ar. This trial does run close to the edge of the mass flow controller's capabilities, so an uneven flow of Ar could have been present and obscure these results. One trial with SF_6 based chemistry was attempted and showed similar selectivity to the CF_4 based recipes. Should CF_4 conditions be either incompatible with some future feature of the sample or never reach an operable rate and selectivity, further experimentation could use this trial as a starting place.

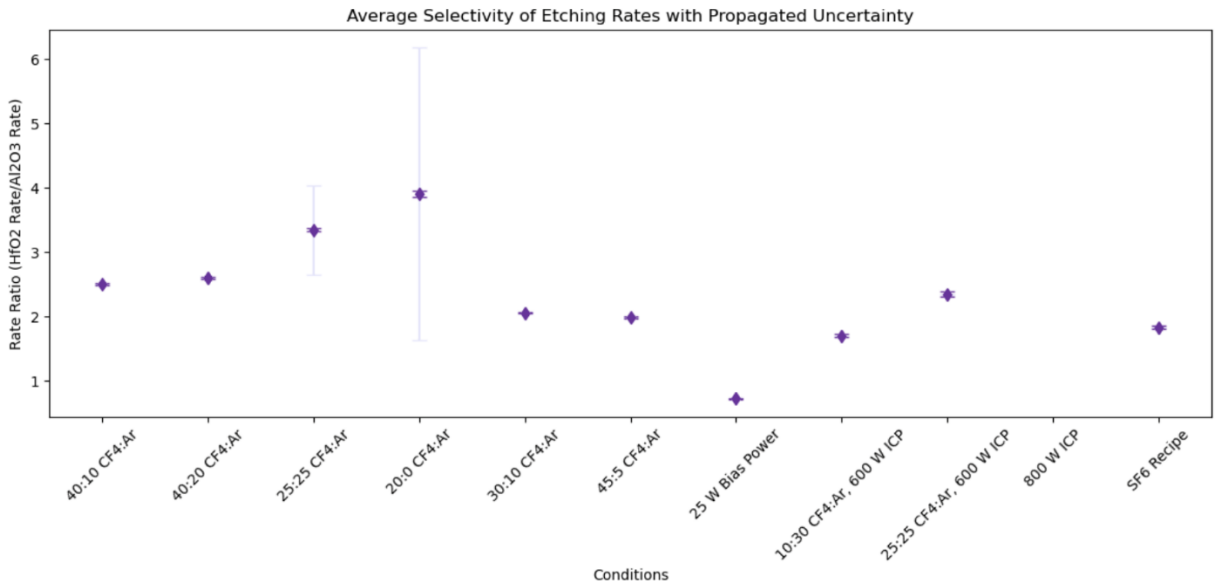

Figure 5. Etch conditions were varied in order to find the largest selectivity between hafnia and alumina.

Changing the ratio of ICP/bias power influences both the uniformity and speed of the etch, so while the selectivity was evaluated in this case, further trials could also look at the anisotropy of the etch. The energy and directionality of the particles will, in part, determine the quality of the nanodisk's sidewalls, essential for the desired optical properties. Decreasing the bias power, lowering the voltage between the sample and plasma, resulted in the lowest selectivity observed, directing trials towards higher ICP powers with a constant 50 W bias power. Increasing the ICP power to 600 W from the original 400 W did not show particularly favorable selectivity and increasing to 800 W etched the alumina film entirely at 120, 60, and 30 second main etch times, so no conclusion could be drawn regarding the selectivity. As none of the power ratios significantly improved the selectivity from the starting 400 W ICP to 50 W bias power, the final stack maintained those conditions. Resolution of the structures could spark a return to this set of experiments, where the etch rates established here could guide the deposited thickness.

2.4 Patterning HSQ using Electron Beam Pattern Generator (EBPG):

The planar lattice features of the metasurface are patterned through e-beam exposure of HSQ. After the deposition of alumina-hafnia on a quartz substrate, we washed and sonicated (2 mins) the sample with acetone and IPA. This helped remove contaminants on the surface of the sample, allowing stronger adhesion of the e-beam resist.

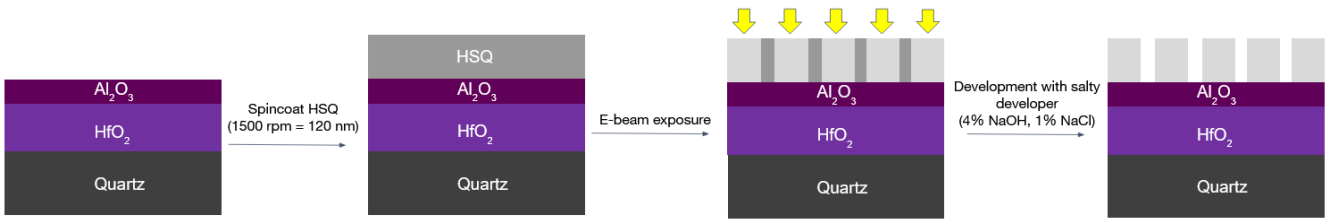

Figure 6: Schematic showing the e-beam exposure of spin-coated HSQ

The sample prep before the e-beam write includes cleaning the sample surface (acetone, IPA, drying using inert gas) and baking a thick layer of HSQ on top of our sample. For the e-beam write, the required parameters were chosen after consulting lab members who fabricate cylinders using HSQ (on other materials). We chose a 1 nA beam current, a beam step size of 5 nm, and applied Proximity Effect Correction (PEC) to avoid overexposure. We also performed a dose sweep between 3000 -9000 uC/cm^2 for every pattern. After the e-beam exposure, the unexposed HSQ is removed from the samples through treatment with a salty developer, a 4% sodium hydroxide (NaOH) and 1% sodium chloride (NaCl) solution. Post-development, the HSQ mask would be left on the sample and ready to be etched, as explained in the last section. A detailed step-by-step procedure for the e-beam part has been outlined in the SOP section of the lithographic patterning of the HSQ.

2.5 Overall process flow:

The analysis of the etch trials showed that we achieved etch selectivity up to 7 with no argon gas (20:0 CF_4:Ar); however, these results were not reproducible later in our trials. Therefore, we chose the second-best etch selectivity (~ 2.6) condition (25:25 CF_4:Ar), which was highly repeatable and consistent over 3 minutes of etching. For a target hafnia film of 40 nm, we deposited 19 nm of alumina, which was 1.2x more than what we required with our most repeatable etch selectivity. This is done because the final etch is generally performed with 10-20% extra time. With these parameters, we deposited the stack on piranha-cleaned quartz substrate using the same conditions as the ones used for deposition for the etch test wafers, as shown in Table 4:

	HfO_2	Al_2O_3
Time (s)	1282	2200
Thickness (nm)	40	19
Dep rate (nm/s)	0.031	0.01

Table 4. Final stack deposition parameters.

Post-deposition, we proceeded with the e-beam exposure, for which we created our mask pattern using an IC layout editor (KLayout) as shown in Figure 7. We use the e-beam parameters described in the SOP and run it on EBPG 1/2 in SNSF to pattern our HSQ mask.

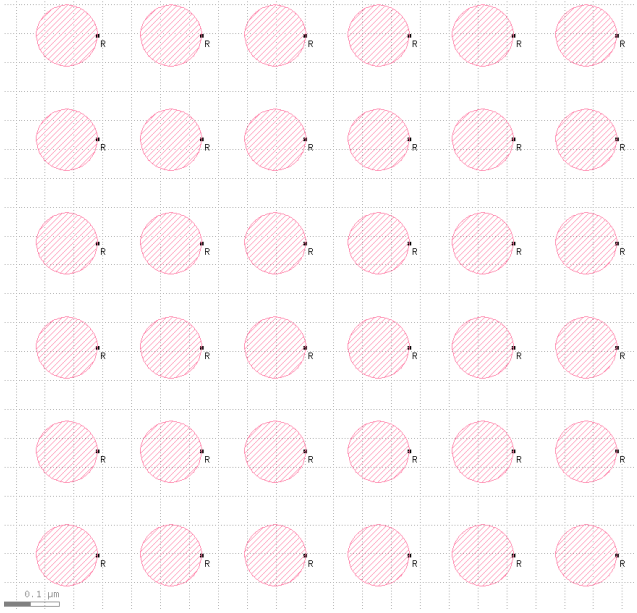

Figure 7: Zoomed image of the pattern file on KLayout.

Next, we developed the sample using our salty developer as outlined in the SOP, which removes unexposed HSQ; Figure 8 shows an SEM of a cropped region of our developed sample.

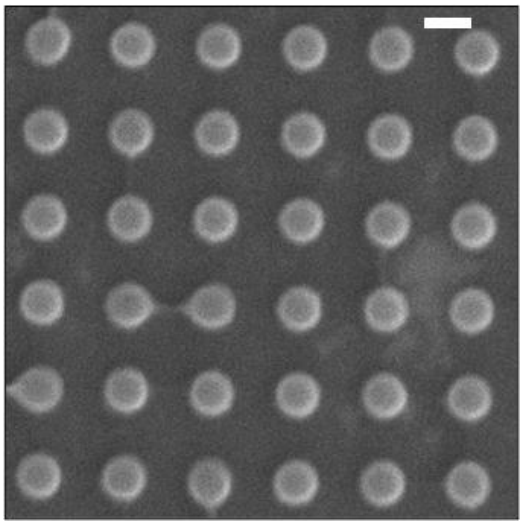

Figure 8: SEM image showing top view of HSQ pillars post-developement. White scale bar: 100 nm.

Next, we etched the developed sample in Cl-based chemistry for 6 seconds, which ideally should leave behind alumina pillars with a thin layer of HSQ on top. To ensure we timed the F-etch perfectly, the excess HSQ was removed by treating the sample in 50:1 HF solution for 40 seconds and rinsed with DI water immediately. Such a short time frame ensures the HSQ is removed but not the entire stack. Figure 9

shows an SEM of a cropped region of our sample after HF removal. The tilted and top view match the HSQ mask design very reasonably.

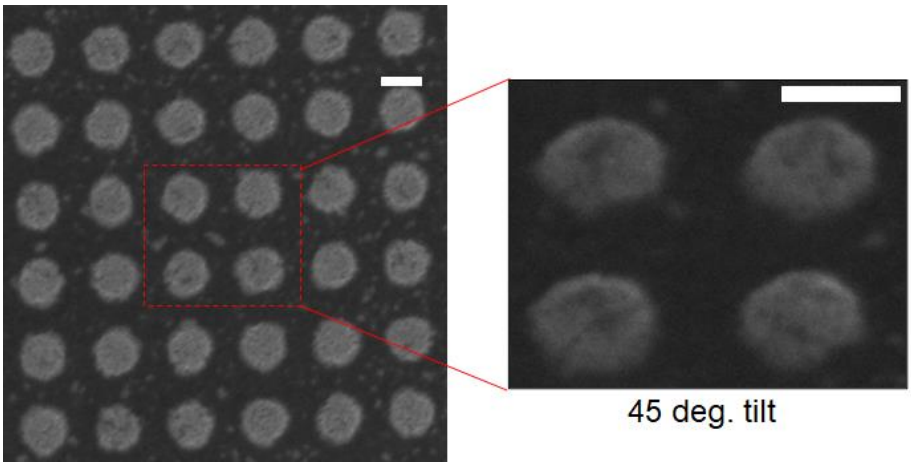

Figure 9: SEM image showing top and tilted zoomed view of alumina pillars after HSQ removal and Cl-based etching. White scale bar: 100 nm.

Next, we etched our sample in F-based chemistry using the parameters for the 25:25 CF_4:Ar gas ratio (selectivity ~ 2.6) for 130 seconds, which was expected to etch all of the alumina and left only hafnia behind. Figure 10 shows an SEM of a cropped region of our sample after F-etching.

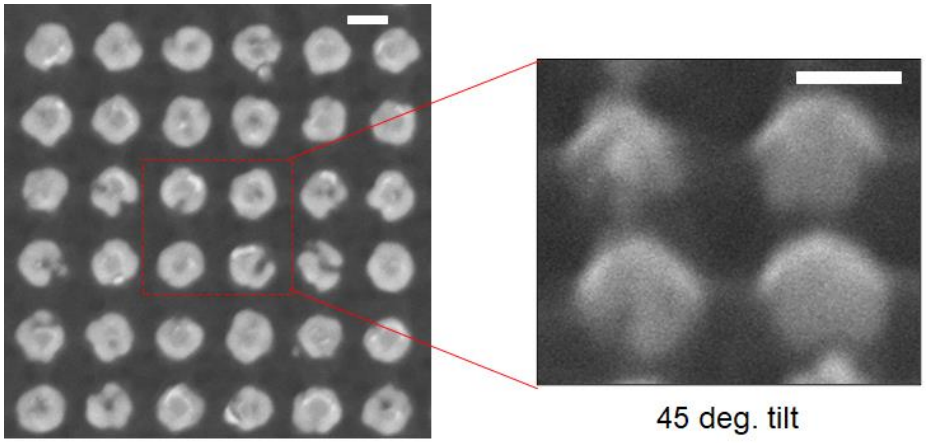

Figure 10: SEM image showing top and tilted zoomed view of hafnia structures after F-based etching. White scale bar: 100 nm.

It clearly showed signs of over-etching because we could not distinguish the sides of the nanodisks. This indicated that the extra alumina deposition did not perfectly match up with the chosen F-etch time. But the process successfully transferred the pattern onto the final hafnia layer, and now we need to fine-tune our etch recipes for better anisotropy and directionality.

3. Conclusion:

3.1 Future optimization:

The work recorded here represents a foundation for fabricating HfO_2 metasurfaces. Initial imaging demonstrates that the established conditions do produce structures; the data collected guides immediate next steps and illuminates some longer term considerations. The next attempt to produce hafnia nanodisks will increase the height, radius, and lattice parameters of the structures, decrease the time of the Fl-based etch step (relatively), and slightly adjust the ICP bias ratio for improved directionality. In the longer term, other resists could be considered, such as ma-N, which may be capable of acting as a hard mask without alumina. This removes pressure to control the etching process with precise timings or potentially leave alumina on the structures, should the timing be underestimated. Alternative process flows could also be considered, such as deposition and patterning of PMMA or another positive resist on HfO_2, evaporation of aluminum or alumina, removal of the resist, Fl-based etching, and finally a wet etching liftoff step in KOH or an appropriate weak acid to remove Al or Al_2O_3 but not HfO_2.

3.2 Conclusion:

Light-matter interaction can be strongly enhanced through arrays of subwavelength-scale nanodisks (metasurfaces), with vast applications in enhancing many physical and chemical processes. Electron beam lithography provides us with a way to fabricate such intricate nanoscale structures with precision. Our project aimed to tackle the problem of fabricating hafnia (HfO_2) metasurfaces designed to enhance light-matter interaction in the UV regime by using alumina as a hard mask in dry-etching conditions. We utilized RF magnetron sputtering on Lesker2 to deposit films of the required thickness (confirmed by profilometry) and build our proposed stack. Using ICP RIE etching in PT-MTL, we developed robust etch recipes that provided reliable etch selectivities to pattern alumina using HSQ (Cl-based recipe) and hafnia using alumina (F-based recipe). One of the significant takeaways was understanding the dependence of the ICP-to-Bias power ratio along with tuning chemical and physical etching through gas (Cl-/F- based) with inert gas (Ar) ratios on the etch selectivity.

In our final stack, we successfully transferred the pattern from HSQ to alumina using Cl-chemistry. However, we over-etched in the F-based etch step, and the final pattern did not have well-defined walls. Our future work involves improving our etch directionality and anisotropy using all the learnings from our etch selectivity tests. Moreover, our project also helped us develop a quick and reliable film thickness characterization method using Sharpie lines and Kapton tape depending on the thickness of the film, which is especially important when ellipsometry fits are unreliable. Lastly, we hope our project report and subsequent SOPs established in our processes help future projects in SNF develop more advanced patterning techniques for hafnia.

3.3 Budget:

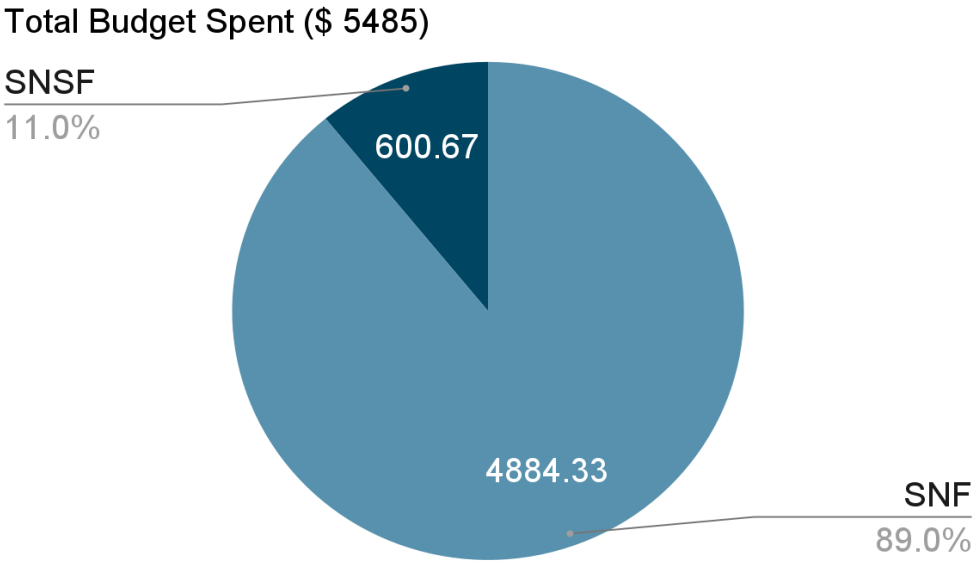

Resources spent within the SNF were divided between trainings ($975.00), supplies including wafers ($127.00), and instrument time on the woollam, Lesker1 and Lesker 2, PT-MTL, and webflex-corr ($3,782.33). E-beam costs are accrued in the SNSF ($600.67).

References:

1. Solomon, M.; Saleh, E.; Poulikakos, L. V.; Abendroth, J. M.; Tadesse, L. F.; Dionne, J. A. Nanophotonic Platforms for Chiral Sensing and Separation. 2020, 53 (3), 588–598. https://doi.org/10.1021/acs.accounts.9b00460.
2. Solomon, M. L.; Hu, J.; Lawrence, M.; García-Etxarri, A.; Dionne, J. A. ENANTIOSPECIFIC Optical Enhancement of Chiral Sensing and Separation with Dielectric Metasurfaces. ACS Photonics 2018, 6 (1), 43–49. DOI:10.1021/acsphotonics.8b01365.
3. Ciriani, M.; Oliveira, R.; Afonso, C. A. Semi-Continuous and Continuous Processes for Enantiomeric Separation. Green Chemistry 2022, 24 (11), 4328–4362. DOI:10.1039/d1gc03668h.
4. Pan, F.; Dixon, J.; Sahil Dagli; Dionne, J. A High-Quality-Factor Chiral Metasurface for Valley-Polarized Emission and Chiral Exciton-Polaritons. 2023. https://doi.org/10.1364/cleo_fs.2023.ff2d.6.
5. Vinod, A.; Mahendra Singh Rathore; N. Srinivasa Rao. Effects of Annealing on Quality and Stoichiometry of HfO2 Thin Films Grown by RF Magnetron Sputtering. Vacuum 2018, 155, 339–344. https://doi.org/10.1016/j.vacuum.2018.06.037.
6. Callister, W. D.; Rethwisch, D. G. Materials Science and Engineering; 2010.
7. Richa Padhye; Adelia; Tunega, D.; Pantoya, M. L. Fluorination of an Alumina Surface: Modeling Aluminum–Fluorine Reaction Mechanisms. ACS Applied Materials & Interfaces 2017, 9 (28), 24290–24297. https://doi.org/10.1021/acsami.7b05372.
8. Kim, J.-W.; Kim, Y.-C.; Lee, W.-J. Reactive Ion Etching Mechanism of Plasma Enhanced Chemically Vapor Deposited Aluminum Oxide Film in CF4/O2 Plasma. Journal of applied physics 1995, 78 (3), 2045–2049. https://doi.org/10.1063/1.360181.

Selected Fluorine and Chlorine-based Etching Recipes:

RD-HfO2 etch					
Step:	**HFO GSa**	**HFO L1a**	**HFO Mb**	**Pump Detach 1**	**Pump Detach 2**
Time	10	3	VARIABLE	20	20
Pressure:	20	20	20	10	0
Ar	00	0	25	0	0
CF4	20	20	25	0	0
N2	0	0	0	25	0
He Cooler Pressure	4000	4000	4000	0	0
Bias RF Power	0	100	50	0	0
ICP RF Power	0	600	400	0	0
Bias Match Load	55				
Bias Match Tune	62				
ICP Match Load	30	30	0	0	0
ICP Match Tune	60	50	0	0	0
Temp Electrode	20	20	20	20	20
Temp Lid	90	90	90	90	90
Temp Liner	70	70	70	70	70
Temp Spool	90	90	90	90	90

RD_Clbased					
Step:	Al GS L	Al Strike	Al ME	Pump Detatch 1	Pump Detatch 2
Time	10	3	1.2	20	20
Pressure:	7	7	7	10	10
Cl2	70	70	70	0	0
BCl3	20	20	20	0	0

N2	0	0	0	25	0
He Cooler Pressure	4000	4000	4000	0	0
Bias RF Power	0	200	150	0	0
ICP RF Pwer	0	1000	1000	0	0
Bias Match Load	55	0	0	0	0
Bias Match Tune	62	0	0	0	0
ICP Match Load	30	0	0	0	0
ICP Match Tune	60	0	0	0	0
Temp Electrode	20	20	20	20	20
Temp Lid	90	90	90	90	90
Temp Liner	70	70	70	70	70
Temp Spool	90	90	90	90	90